Evolution of Low-Profile Ultra-Wideband Frequency Selective Surface with a Stable Response and Sharp Roll-Off at Lower Band for C, X and Ku Band Applications

Anik Naha BISWAS[1], Suparna BALLAV[1], Ayan CHATTERJEE[2], Susanta Kumar PARUI[1]

[1]Dept. of ETC, Indian Institute of Science Engineering and Technology, Shibpur, Howrah, West Bengal, India
[2]Dept. of ECE, National Institute of Technology Sikkim, Ravangla, South Sikkim, India

anahabiswas@gmail.com, ballav.suparna@gmail.com, ayanmrinal26@gmail.com, arkapv@yahoo.com

Submitted August 12, 2019 / Accepted May 16, 2020

Abstract. *This paper focuses on two different design flows of how an ultra-wideband FSS can be achieved from a narrowband structure. By amalgamating a capacitive patch with a corrugated square slot structure, as the first approach while the second approach involved designing a dual layer FSS by etching the corrugated square slot at both top and the bottom layer of the substrate. A 98% bandwidth extending from 5.5 GHz to 16 GHz was achieved using the first approach while the modified structure yields about 107% bandwidth covering up the entire range from 5 GHz to 16.5 GHz, hence improving the performance in terms of bandwidth. The final modified FSS structure manifests the polarization insensitive nature as well as angle insensitivity up to 60° angle of incidence in terms of the entire range of the wide reflection band, and covering all the three bands (C, X and Ku band). The transmission coefficient manifests a stable response below 20 dB almost throughout the entire band without significant variation. The measured result shows good agreement with the experimented result validating the fabricated prototype and measurement. The bandwidth can be tuned by varying different parameters like corrugation dimension, dielectric permittivity, substrate height which have been explained in this paper.*

Keywords

Frequency Selective Surface (FSS), ultra-wideband, corrugation, polarization insensitive, roll-off factor, quality-factor

1. Introduction

FSS is a sort of spatial filter which evinces both bandpass (aperture or grid type) and bandstop (patch type, cross type, slot type) responses based on the structure of the unit cell [1–4]. Various studies and research works have been carried out on FSS for its diverse applications in antenna gain enhancement, microwave absorber, polarization conversion, shielding purpose. Satellite communication is a disruptive technology in modern science and day by day the applications of satellites are increasing so rapidly from the field of radio communication to weather forecasting, astronomy, programs broadcasting, navigation etc. At present, the rising demand of wideband Frequency Selective Surface (FSS) application in satellite communication at X, Ku, K bands has caught the interest of the scientists. But as the satellite communication technology is flourishing, the lower frequency bands (L, S, C bands) are getting congested which is a serious problem in recent days. So, nowadays, the higher frequency bands (X band, Ku band) are in high demand for the purpose of satellite communication [5]. Nowadays, ultra-wideband application has gained ample attention because of the unlicensed spectrum (3.1 to 10.6 GHz) declared by Federal Communication Commission (FCC) [6]. FSS may exhibit one or more resonant frequencies (multiband FSS) based on the number of metallic layers, the unit cell structure and its corresponding equivalent circuit [7–9]. In order to accomplish infinite array characteristics with finite array of FSS elements and to operate the FSS in a lower frequency range, the imperativeness of miniaturization of unit cell size is inevitable [10]. The researchers have achieved significant progress on angle sensitive wideband FSS since B. A. Munk has mentioned how angular stability can be improved by reducing inter element spacing [1]. Wideband FSS can be used to provide broadband characteristics to spatial filters, absorbers, antennas in order to improve their responses [11–13].

A new FSS design methodology for ultra-wideband application was proposed in [14]. It consists of an array of two different patch elements – one square loop and one crossed dipole – associated with each other in a single unit cell, to enhance the bandwidth of each individual patch analyzed separately, hence achieving a bandwidth of almost 52.4%. A very wideband, low-profile, single layer FSS reflector, by designing the unit cell with a cross-dipole and a ring etched on the opposite surfaces of a single substrate layer of FR4 material was investigated in [15]. The structure evinces a wide stopband of 7.5 GHz extending from 6.5 GHz to 14 GHz with a linearly decreasing phase over the entire bandwidth. In [4], a cascaded dual-layer patch type wideband FSS reflector etched on separate layers of FR4 substrate was designed which exhibits a wide stopband of maximum 10.4 GHz ranging from 5.2 GHz to 15.6 GHz with two layers in cascade. A dual-layer low-profile ultra-wideband FSS with two FR4 substrates comprising one cross dipole and a slot at the top surface and a similar structure with one slit inserted to the metal frame in between two dielectric materials was proposed and experimentally validated in [16]. The structure operates at C and X bands having 106% bandwidth with a range from 3.5 GHz to 11.45 GHz. In [17], a modified design was presented to accomplish an ultra-wideband FSS reflector with a single layer for microwave application. The unit cell comprises a square loop and a ring printed on both side of FR4 substrate providing a wide reflection band of almost 12 GHz ranging from 5.24 GHz to 17.18 GHz with a stable frequency response up to 45° angle of incidence. A three order ultra-wideband bandpass FSS comprising a patch array, a lattice array with transmission line (medium layer) in between them has been proposed which exhibits 50% pass band extending from 7.79 GHz to 12.49 GHz [18].

In this paper, a gradual improvement in the bandwidth with different FSS structures has been studied. In order to accomplish a very wide bandwidth, we have merged a conventional narrowband patch type FSS with a corrugated FSS structure with square loop without altering the dimensions. This combined structure provides more improved and wider bandwidth than that of the previous structures due to the addition of an additional inductance in parallel coming into picture by virtue of the conducting patch. Another way to obtain wide bandwidth has been proposed in this paper. The final FSS unit cell is designed with the previously mentioned corrugated square slot placing both side of the dielectric substrate with reduced size of the corrugation. This modified structure upgrades the bandwidth to 107% ranging from 5 GHz to 16.5 GHz covering all the three bands (C, X and Ku band). The transmission coefficients, phase plots for different FSS structure have been simulated using the Finite Element Method magnetic solver High Frequency Structural Simulator (HFSS).

2. Unit Cell Design Methodology

In this section, two different ways of designing ultra-wideband FSS structure have been discussed. At first, one single square slot corrugated structure has been associated with a square patch to constitute an ultra-wideband bandstop FSS. These three FSS unit cell schematic are shown in Fig. 1. In the second approach, the corrugated structure with square loop is etched on both sides of the dielectric substrate which exhibits a very wide bandwidth. Finally, this structure is modified with reduced dimension of the corrugation to obtain lower Q-factor, thus much wider reflection band is achieved. Both the structures are given in Fig. 2. The design parameters are listed in Tab. 1. In all the structures proposed in this paper, the unit cells made of copper are etched on the commonly used FR4 substrate having a dielectric constant of 4.4, a loss tangent of 0.02 and

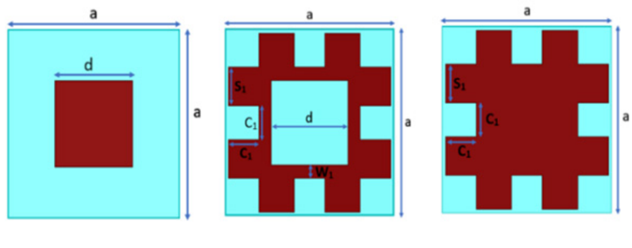

(a) (b) (c)

Fig. 1. Schematic of unit cell of (a) FSS 1, (b) FSS 2, (c) FSS 3.

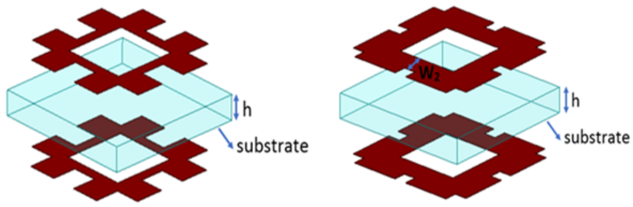

(a) (b)

Fig. 2. Schematic of unit cell of (a) FSS 4, (b) FSS 5.

Parameters	a	S_1	C_1	S_2	C_2	W_1	W_2	d	h
Values (mm)	11	2.3	2	3.8	1	0.8	1.8	5	1.6

Tab. 1. Unit cell design parameters.

a thickness of 1.6 mm which is much smaller than the wavelength corresponding to the smallest frequency (5 GHz) of the wide reflection band of the FSS structure making the substrate much thinner and less bulky. All the proposed structures manifest bandstop responses as their equivalent circuits give an overall capacitive effect which makes them reflective.

3. Equivalent Circuit Model

We can explain the results and the operation of a given structure from its equivalent circuit and the values of the capacitance and inductance. The dielectric substrate is modelled as a short piece of transmission line [14, 19]. The thickness of the substrate is considered as the length of the transmission line. The characteristics impedance of the substrate (modelled as a transmission line) is given by $Z = Z_0/\sqrt{\varepsilon_r}$, where ε_r is the dielectric constant of the FR4 substrate ($\varepsilon_r = 4.4$) and Z_0 is the free space impedance which has a value of 377 Ω. The free space on the two sides of the proposed structure can be viewed as a semi-infinite transmission line whose characteristics impedance can be written as: $Z_{01} = Z_0R_{01}$ and $Z_{02} = Z_0R_{02}$, where R_{01} and R_{02} are the normalized source and load impedance ($R_{01} = R_{02} = 1$). The substrate parasitic capacitance and inductance value can be obtained as [20]: $L_{sub} = \mu_0\mu_r h$ and $C_{sub} = (\varepsilon_0\varepsilon_r h)/2$, where L_{sub} and C_{sub} are the parasitic inductance and capacitance values of the dielectric substrate. We are assuming that the incident wave is x-polarized. Now, FSS 1 consists of a patch type element etched at the top surface of the FR4 dielectric substrate. The array of patch elements gives an overall capacitive effect representing a first order bandstop filter [19].

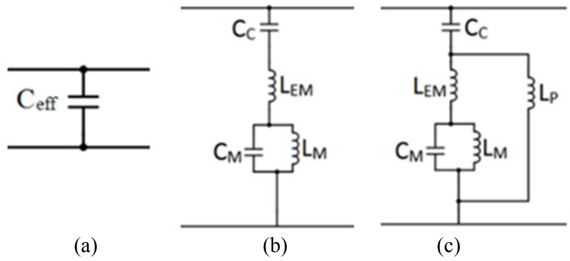

Fig. 3. Equivalent circuit model of (a) FSS 1, (b) FSS 2, (c) FSS 3.

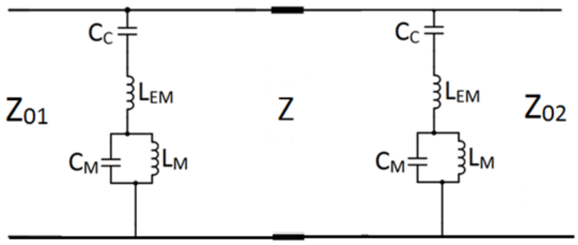

Fig. 4. Equivalent circuit model of FSS 4 and FSS 5.

The equivalent circuit shown in Fig. 3(a) comprises a lumped capacitance which is in parallel with the substrate reactance [20, 21]. In FSS 2, the array of corrugated unit cell with one square loop at the top surface is represented by the equivalent circuit given in Fig. 3(b). The parallel connection of inductance (L_M) and capacitance (C_M) represents the corrugated patterns of the designed FSS structure. The extended metallic portions between which the corrugation is located give rise to an inductance (L_{EM}) which comes in series. An additional coupling capacitance (C_C) is introduced which is connected in series with the parallel combination. This structure operates as a band-reject filter for x-polarized incident wave. The substrate reactance effect comes in parallel with the metallic structure equivalent circuit [22].

Now, the above two structures (i.e. patch and corrugated structure) have been merged to obtain FSS 3 which has been modelled by the equivalent circuit shown in Fig. 3(c). Here, the metallic patch is in parallel with the corrugated structure. So, in this design, another lumped inductance (L_P) due to the conducting patch element has come into the picture which is connected in parallel with the corrugated structure equivalent circuit as shown in Fig. 3(c). The effect of the substrate reactance is in the parallel combination with the proposed equivalent circuit. We have shown another way to procure a wide bandwidth by etching the corrugated metallic structure with one rectangular slot (FSS 2) at both the top and bottom surface of the FR4 substrate. FSS 4 has been modelled by its corresponding equivalent circuit which is shown in Fig. 4. The equivalent circuit is quite similar to that of FSS 2, but in this case the top and the bottom layer are in parallel combination. The equivalent circuit model of the individual layer which is tantamount to that of FSS 2 are connected in parallel in the equivalent circuit representation of FSS 4. The substrate reactance effect has been taken into account as before. Also, in FSS 5, like FSS 4, the corrugated metallic structure with one rectangular slot has been etched on both sides of the substrate, but in this case the dimension of the corrugation has been reduced to 1 mm to improve the bandwidth. So, the equivalent circuit of FSS 5 is similar to that of FSS 4, but the lumped inductance value arising due to the meandered portion is decreased due to reduced dimension of the corrugation. The equivalent circuit modelling for FSS 5 has been done in similar approach used in the previous case. Figure 4 also represents the equivalent circuit of FSS 5.

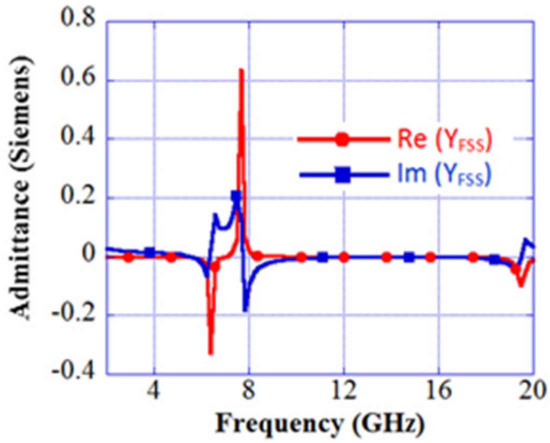

Fig. 5. Simulated overall admittance plot for FSS 5.

The reflection loss is determined by the total effective admittance (Y_{total}) of the structure which is equal to the parallel connection between surface admittance (Y_{FSS}) of both the metallic layers etched on both side of the FR4 dielectric substrate.

$$Y_{\text{total}} = Y_{\text{FSS}} + Y_{\text{FSS}}. \tag{1}$$

The individual layer has a complex surface admittance which equals to Y_{FSS}.

$$Y_{\text{FSS}} = 1/\left[R + \mathrm{j}\left(\omega L - \left(\frac{1}{\omega C}\right)\right)\right], \tag{2}$$

$$Y_{\text{FSS}} = \left[\mathrm{Re}\left(Y_{\text{FSS}}\right) + \mathrm{j}\,\mathrm{Im}\left(Y_{\text{FSS}}\right)\right]. \tag{3}$$

The complex admittance of the FSS can be determined from the lumped parameters (resistance, inductance and capacitance) of the corresponding equivalent circuit. Now, for full reflection, i.e. zero transmission, according to the transmission line theory, the load end should be open circuited (i.e. the load impedance will be very high, ideally infinite). So, in order to obtain the bandstop response, the FSS equivalent circuit impedance has to be very high, or in other words, the effective total admittance will be very low, ideally has to be zero. The overall admittance of FSS 5 is shown in Fig. 5. In this plot, we can see that the magnitude of real and imaginary parts of the FSS admittance are almost zero over the entire bandwidth which substantiates the fact that the FSS structure provides a bandstop response over the entire band.

4. Results and Discussion

The transmission coefficients, phase plots for different FSS structure have been simulated using unit cell boundary condition where Floquet Port excitation was assigned in High Frequency Structural Simulator (HFSS) software. We have plotted the transmission coefficient (S_{21}) curves of three uniplanar FSS (FSS 1, FSS 2 and FSS 3) to represent the improvement of bandwidth using the first method in Fig. 6(a). FSS 1 is a patch type element which gives a stopband of 1.4 GHz ranging from 15.7 GHz to 17.1 GHz (8.5% bandwidth) centered around the resonant frequency at 16.4 GHz. The S_{21} curve has a transmission loss of approximately 20 dB at the corresponding resonant frequency. FSS 2, consisting a single layer of corrugated pattern with one square slot, resonates at 8.1 GHz with a 10 dB reflection band extending from 4.5 GHz to 11 GHz providing near about 84% wide bandwidth with 43 dB insertion loss at 8.1 GHz. By virtue of this corrugation effect, the inductance of the structure gets increased due to increased current path which in turns reduces the resonant frequency and enhances the transmission loss [23]. Later, both the FSSs have been merged to constitute FSS 3 to provide a wider bandwidth than the previous two structures. An additional inductance due to the metallic conducting patch is introduced in parallel which increases the 10 dB reflection band of FSS 3 compared to the FSS 2 reflection bandwidth due to mitigation of overall inductance which in turn reduces the Q-factor of the design (Bandwidth is inversely proportional with Q-factor). In this case, the bandwidth is even greater than the sum of the bandwidth of FSS 1 and FSS 2. This structure exhibits a resonant frequency at 12.7 GHz with a wide stopband of 10.5 GHz ranging from 5.5 GHz to 16 GHz. A significant insertion loss of almost 44 dB is obtained at the resonant frequency. The transmission coefficient phase plots have been presented in Fig. 6(b) for all the uniplanar structures. The S_{21} curve for FSS 1 experiences a large phase transition at the resonant frequency, but it doesn't cross zero degree, the phase always remains negative which indicates that the patch type element has an overall capacitive effect. We can observe a large phase transition of transmission coefficient phase for both FSS 2 and FSS 3 of almost 152° at the respective resonant frequency. In this case, the S_{21} phase changes its value from negative to positive one implying that the structure alters its nature from capacitive to inductive around the resonant frequency. The surface current distribution has been shown in Fig. 7 at three different frequencies for FSS 3. It is conspicuous from the figure that the surface current density at 12.7 GHz which is primarily the resonant frequency is stronger than the other two frequencies inside the wide reflection band. Maximum surface current density is obtained at the edges of the structure, it decreases down from the edge towards the middle of the unit cell. The enlarged current path length compacts the unit cell size. The current distribution plots at the resonant frequency and the edges of the wide reflection band signify that the current flows in the patch throughout the entire band. The transmission coefficient curves for FSS 4 and FSS 5 have been illustrated in Fig. 8(a) to depict the bandwidth enhancement in the second approach. In FSS 4, the current on one metallic layer generates a magnetic field which couples with the metallic layer on other side leading to inductive coupling.

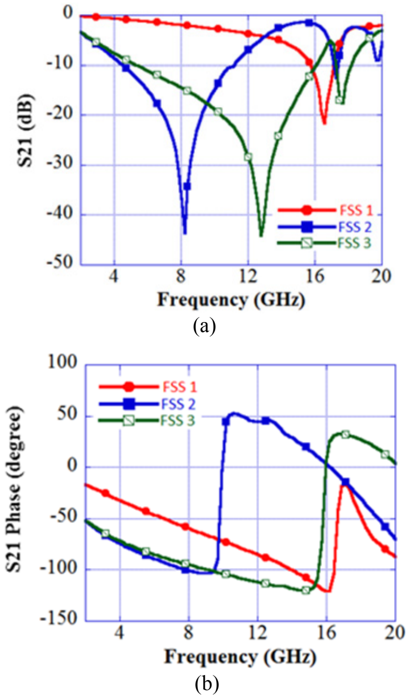

Fig. 6. (a) Simulated transmission coefficient plot of single layer unit cell. (b) Simulated transmission coefficient phase plot of single layer unit cell.

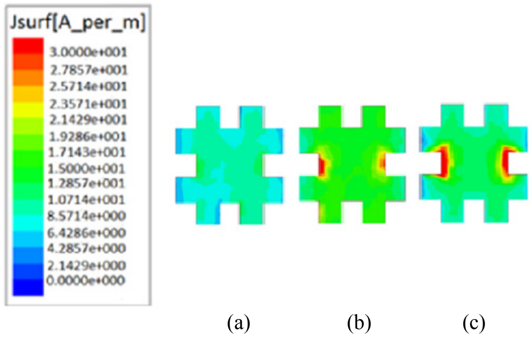

Fig. 7. Surface current distribution of FSS 3 at (a) 5.5 GHz, (b) 12.7 GHz, (c) 16 GHz.

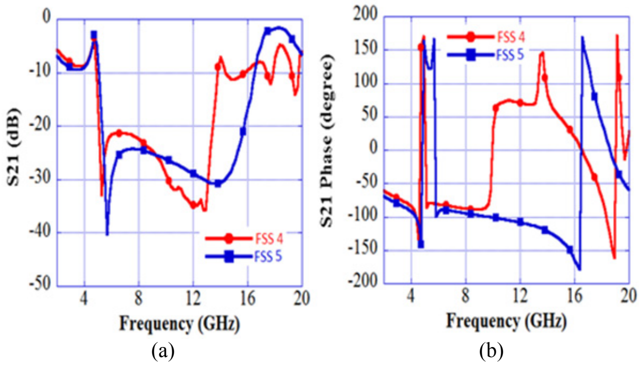

Fig. 8. (a) Simulated transmission coefficient plot of dual layer unit cell. (b) Simulated transmission coefficient phase plot of single dual unit cell.

Capacitive coupling arises due to the metallic layers on the either side of the dielectric substrate. This mutual capacitance and inductance between these two metallic layers isolated by FR4 substrate pose the bandwidth enhancement. The directions of the current on the top and bottom metallic layer are anti-parallel, thus countervailing each other's effect causing resonance. This bi-planar structure results in a very wide stopband of almost 97% covering the range from 4.8 GHz to 13.8 GHz. The bandwidth is ameliorated further with the similar dual-layer structure but truncated dimension of the corrugation. As the dimension is lowered, the effective path for the current flow is mitigated which minimizes the effective inductance, thus lowering the Quality factor of the entire structure which is responsible for the enhancement of the bandwidth. This final structure (FSS 5) evinces an ultra-wide reflection bandwidth which encompasses all the three frequency bands (C, X and Ku) with 107% bandwidth. Figure 8(b) illustrates the transmission coefficient (S21) phase plot of FSS 4 and FSS 5. The transmission coefficient of FSS 5 has a linear decreasing phase over the entire bandwidth.

The transmission coefficient response of FSS 5 has been plotted for different angle of incidence as well as both TE and TM polarized wave in Fig. 9. Lesser the gaps between the neighboring unit cells will be, more angular stability will be achieved. So, the gaps between the consecutive unit cells are kept very small (0.4 mm) in order to maintain the angular insensitivity for different angle of incidence. The 10 dB reflection bandwidth remains almost constant for the different incident angles up to 60° for both TE and TM polarized incident wave. Beyond 45° angle of incidence, multiple resonance results in slight enhancement of bandwidth. For a particular incident angle, the S_{21} response for both TE and TM mode are tantamount to each other. So, we can say that the final proposed dual layer structure is polarization independent in terms of wide bandwidth.

Roll-off factor in any filter circuit is defined as steepness of the transmission coefficient curve in the transition of passband and stopband. It is measured as a logarithmic function having a unit of decibel per gigahertz (dB/GHz). The roll-off rate ζ is computed by the following equation [24]:

$$\zeta = \frac{\alpha_1 - \alpha_2}{f_1 - f_2} \tag{4}$$

where α_1 and α_2 are 10 dB and 30 dB attenuation point respectively where as f_1 and f_2 are the frequencies at that corresponding attenuation point. From Fig. 8(a), we can estimate the average sharpness factor of roll-off rate of the S_{21} curve for FSS 5 as 43.5 dB/GHz at lower band which indicates a sharp roll-off at the lower edge of the ultra-wide reflection band because of meandering effect as well as dual layer configuration and 9.1 dB/GHz at upper band which achieves a relatively low selectivity. A stable flat response throughout the band can be accomplished with this final modified dual layer structure.

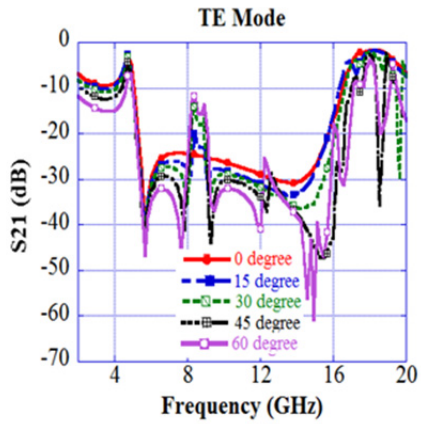

(a)

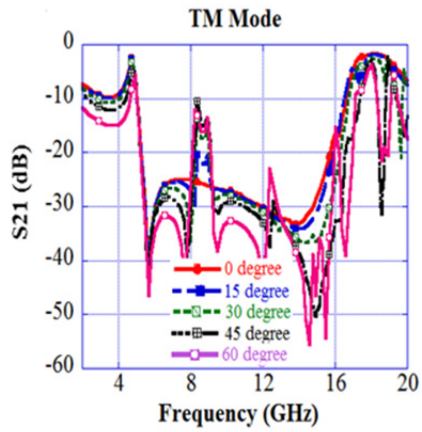

(b)

Fig. 9. (a) Simulated transmission coefficient plot of FSS 5 for (a) TE polarization, (b) TM polarization.

5. Parametric Analysis

The effects of different imperative parameters like meander dimension, substrate height, dielectric permittivity which control the bandwidth of the final modified structure (FSS 5) have been delineated in this section. We have preferred the above-mentioned values of distinctive parameters to design this structure for making it applicable in practical scenario.

5.1 Effects of Dimension of the Corrugation

Figure 10 shows the variation of the reflection bandwidth with the width of the meandering for FSS 5. Lesser the width will be, more will be the bandwidth and vice-versa. We have provided different transmission coefficient plots for different width ranging from 1 mm to 2.5 mm with a linear increasing step of 0.5 mm. We can clearly observe that the bandwidth is gradually decreasing as we are heading towards higher width of the corrugation. The enlargement of the dimension will cause the current to travel a longer path which will rise the inductance and thus lessening the obtained 10 dB bandwidth.

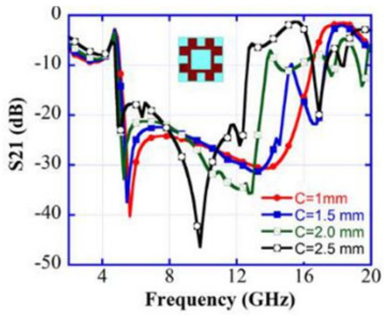

Fig. 10. Simulated result illustrating the variation of S_{21} parameters of FSS 5 for different width of corrugation.

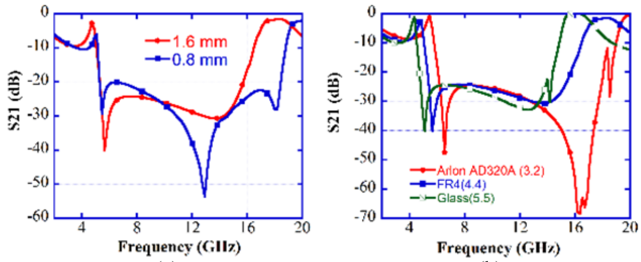

(a) (b)

Fig. 11. Simulated result illustrating the variation of S_{21} parameters of FSS 5 for: (a) different substrate thickness, (b) different dielectric material.

5.2 Effects of Substrate Height

The substrate height is another important parameter which can steer the bandwidth of the FSS structure. We have considered two easily available substrate thicknesses (0.8 mm and 1.6 mm) in our study. The 10 dB reflection bandwidth is inversely proportional to the height of the dielectric substrate. When considering 0.8 mm height of the substrate instead of 1.6 mm, the bandwidth is a bit higher. The broadening of substrate thickness mitigates the coupling capacitance between the top and bottom metallic layers whereas enhances the inductive coupling at the same time. By virtue of this phenomenon, the reduction and the enhancement in overall capacitance and inductance respectively cause the bandwidth to constrict. But the better angular stability obtained with 1.6 mm thickness makes us inclined to the greater substrate height. So, we have made a trade-off between the bandwidth and the angular stability which is acceptable in practical application. This study has been presented in Fig. 11(a).

5.3 Effects of Dielectric Permittivity

The dielectric permittivity of the substrate also plays a vital role in determining the reflection bandwidth of this proposed FSS design. We have simulated the transmission coefficients for different permittivity and presented this parametric study in Fig. 11(b). We have chosen Arlon AD320A, FR4 and glass material possessing a permittivity of 3.2, 4.4 and 5.5 respectively for conducting our study to observe the variation of the bandwidth. The 10 dB reflection bandwidth will get narrower with the use of the substrate material with higher dielectric constant. Higher dielectric permittivity will reduce the fringing fields which will diminish the fringing capacitance value [25]. More the dielectric constant will be, less will be the dielectric loss of the substrate ($Q_d = (\omega_0\varepsilon)/\sigma = (\tan\delta)^{-1}$). These two phenomena will ensue the enhancement of overall quality factor which in turn reduces the 10 dB reflection bandwidth. We can achieve greater bandwidth with Arlon AD320A, but we have fabricated using FR4 substrate due to unavailability of Arlon320A in our laboratory. This design could be implemented using Arlon320A material to obtain almost 113% bandwidth covering all the three frequency bands (C, X and Ku).

6. Fabrication and Measurement of FSS Prototype

To validate the simulated results, a large FSS prototype of 77 mm × 77 mm consisting of 7 × 7 unit cells has been fabricated by etching the metallic layers on both side of FR4 dielectric substrate. The waveguide measurement method has been carried out to verify the S_{21} parameters of the fabricated prototype. We have used three different types of waveguide to measure the entire ultra-wide bandwidth. The C band is measured by a standard waveguide having an aperture of 47.5 × 22 mm^2 whereas the X and Ku band have been measured by the standard waveguides with an aperture size of 23 × 11 mm^2 and 16.5 × 8.5 mm^2 consecutively.

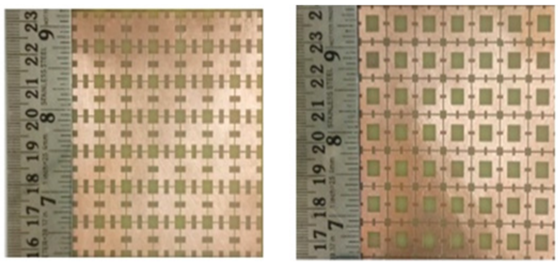

(a) (b)

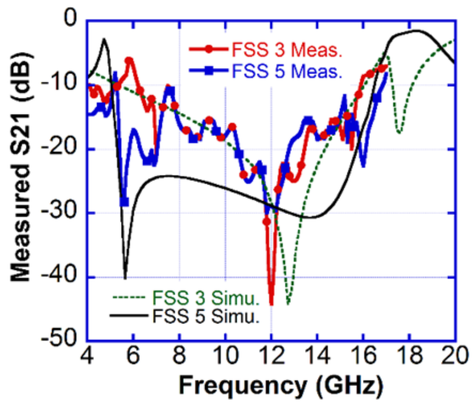

(c)

Fig. 12. (a) Fabricated prototype of FSS 3. (b) Fabricated prototype of FSS 5. (c) Measured transmission coefficient response.

Reference	Design Type	Unit Cell Design	Bandwidth (GHz)	Unit Cell Size	Roll-off Rate (dB/GHz)
Proposed	Uni Planar Design	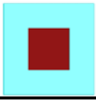	15.7 – 17.1 (8%)	0.58λ	14.3 at lower band and 20 at upper band
			4.5 – 11 (84%)	0.16λ	6.25 at lower band and 7.81 at upper band
		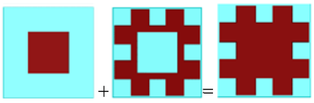	5.5 – 16 (98%)	0.2λ	2.91 at lower band and 7.41 at upper band
	Both Sided Copper Cladded Substrate (Polarization Insensitive)	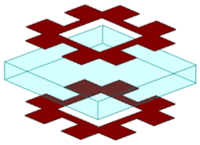	4.8 – 13.8 (97%)	0.18λ	44.12 at lower band and 25 at upper band
		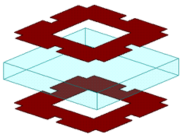	5 – 16.5 (107%)	0.18λ	43.5 at lower band and 9.1 at upper band
[4]	Uni Planar Design	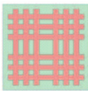	5.2 – 15.6 (100%)	0.3λ	60 at lower band and 6.25 at upper band
[14]	Uni Planar Design	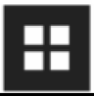	6.7 – 11.5 (52.4%)	0.3λ	8.7 at lower band and 13.33 at upper band
[15]	Both Sided Copper Cladded Substrate	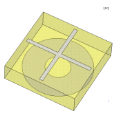	6.5 – 14 (73%)	0.26 λ	50 at lower band and 28 at upper band
[16]	Dual Layer Design	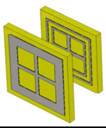	3.5 – 11.45 (106%)	0. 175λ	28.6 at lower band and 13.33 at upper band
[27]	Both Sided Copper Cladded Substrate (Polarization Sensitive)		8.4 – 12.4 GHz for TE Polarization and 12.4 –15.8 GHz for TM Polarization	0.21λ	40 at lower band and 13.33 at upper band

Tab. 2. Comparison with previous works for bandstop UWB FSS.

The measurement has been performed with two waveguides of each type which were connected to an Agilent N5230A vector network analyzer through coaxial cables. The S_{21} coefficient is measured using the vector network analyzer. The fabricated prototype was placed between two waveguides and hold tightly so that the whole energy is reflected from the bandstop FSS. At first, the measurement was conducted with only two waveguides in the absence of FSS prototype and then FSS was engraved in between two waveguides. The free space results were subtracted from the results obtained with the fabricated sample to accurately plot the transmission coefficient curve of the FSS. The measured and simulated results for both FSS 3 and FSS 5 have been illustrated in Fig. 12 and they are in good agreement. In case of both FSS 3, the lower edge of the measured stopband starting from 6 GHz shifts slightly towards the higher frequency in comparison to the simulated result whereas the upper edge crosses –10 dB near 16 GHz, but the measured resonant frequency nearly matches with the simulated one. The measured transmission loss is analogous to the simulated S_{21} deep which in turn validates our design. For FSS 5, the measured result of

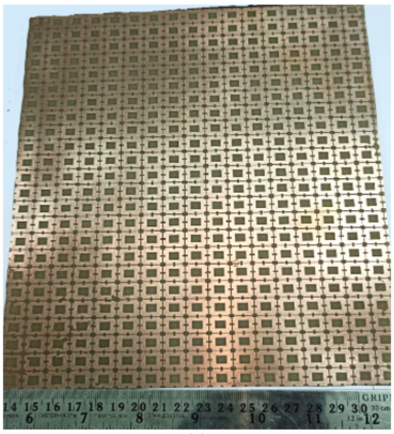

(a)

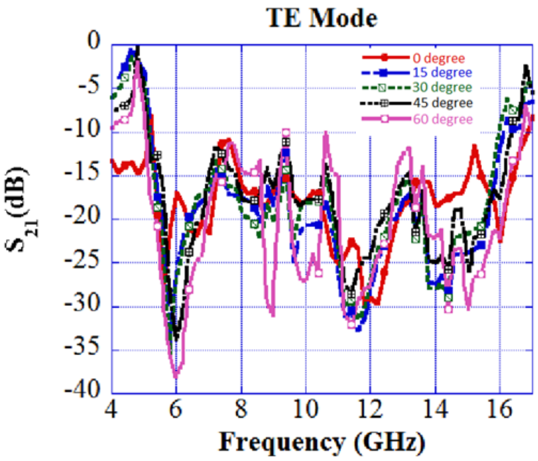

(b)

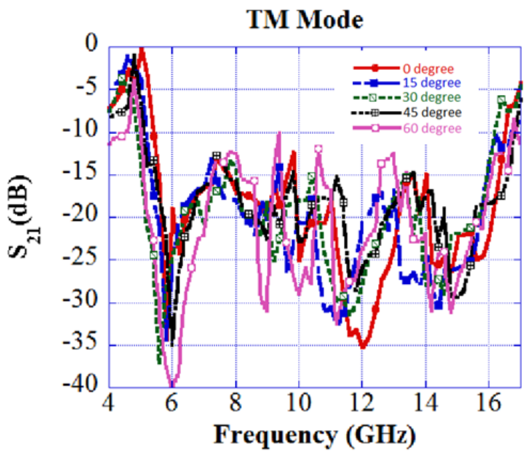

(c)

Fig. 13. (a) Larger (24 × 17) fabricated prototype of FSS 5. (b) Measured transmission coefficient plot of FSS 5 for TE polarization. (c) Measured transmission coefficient plot of FSS 5 for TM polarization.

the fabricated prototype justifies our claim of procuring an ultra-wide reflection bandwidth of 11.5 GHz with a small shift of 6% for the lower edge (starts from 5.3 GHz) of the band. The slight deviation between the measured and the simulated results arises due to some unavoidable reasons like fabrication error, scattering of EM waves and the reflection from the edges [4, 26]. A vivid comparison of this proposed ultra-wideband FSS with the previous works has been provided in Tab. 2. We can incontrovertibly conclude from the data listed in the table that our design achieves comparatively wider bandwidth, much lower profile, compactness and good polarization insensitivity than the other established works. A much larger prototype of FSS 5 (24 × 17) has also been fabricated in order to carry out the measurement of transmission coefficient at distinct angle of incidence to substantiate the simulated result provided in Fig. 9.

The fabricated structure was placed in between two horn antennas and positioned at far-field distance with respect to each antenna. The experiment was conducted using three different pair of horns for three distinguished operating bands (C band, X band and Ku band). The free space measurement was performed only with two horn antennas in the absence of the fabricated FSS prototype. The measured results illustrated in Fig. 13 matches well with the simulated one which ascertains the veracity of the proposed design performance.

7. Conclusion

Two different techniques of achieving ultra-wideband FSS have been presented vividly in this article. In the first method, we introduced an inductor in parallel by amalgamating the corrugated square slot with the square patch to broaden the reflection bandwidth by virtue of the mitigation of overall inductance. In the second procedure, we placed the corrugated square slot at both sides of the substrate which incorporates an additional mutual inductance and capacitance between the two layers and then diminished the width of the meanders in order to abate the inductive effect so as to obtain an ultra-wideband of 11.5 GHz. The final proposed and fabricated structure widens the reflection bandwidth from 5 GHz to 16.5 GHz offering approximately 107% bandwidth subsuming the three radio-frequency bands (C band, X band and Ku band). X band is primarily used by the military for defense purpose. The Ku band is used for direct broadcast satellite services, distance learning application etc. where downlink frequency varies between 10.9 GHz to 12.75 GHz and uplink frequency is 14 GHz. This FSS structure can be used in ground penetrating radar in C band whereas it becomes utilitarian in defense sector as radome for its X band application and its stable response for nearly the entire band. Due to the sharp roll-off at the lower edge of the ultra-wideband, it is advantageous in terms of stopband rejection and high frequency selectivity. The bandstop response can be utilized for gain enhancement of satellite antenna operating in these three microwave frequency bands.

Acknowledgement

The authors are highly obliged to the Ministry of Human Resource and Development (MHRD) for valuable financial support.

Reference

[1] MUNK, B. A. *Frequency Selective Surfaces: Theory and Design*. New York (USA): John Wiley, 2005. ISBN: 9780471723776

[2] MUNK, B. A. *Finite Antenna Arrays and FSS*. John Wiley, 2005. ISBN: 9780471457534

[3] ZHU, H., YU, Y., LI, X., et al. A wideband and high gain dual-polarized antenna design by a frequency selective surface for a WLAN applications. *Progress In Electromagnetics Research C*, 2014, vol. 54, p. 57–66. DOI: 10.2528/PIERC14072801

[4] SARIKA, TRIPATHY, M. R., RONNOW, D. A wideband frequency selective surface reflector for 4G/X-band/Ku-band. *Progress In Electromagnetics Research*, 2018, vol. 81, p. 151–159. DOI: 10.2528/PIERC18010908

[5] SKOLNIK, M. I. *Introduction to Radar Systems*. *Radar Handbook 2*. Mc Graw Hill, 1962. ISBN: 0-07-057909-1

[6] JINDAL, P., YADAV, A., SHARMA, S. K. Dual stop band frequency selective surface for C and WLAN band applications. *AEU-International Journal of Electronics and Communications*, 2018, vol. 97, p. 267–272. DOI: 10.1016/J.AEUE.2018.10.016

[7] REED, J. A., BYRNE, D. M. Frequency-selective surfaces with multiple apertures within a periodic cell. *Journal of the Optical Society of America A (JOSA A),* 1998, vol. 15, no. 3, p. 660–668. DOI: 10.1364/JOSAA.15.000660

[8] SEN, G., MANDAL, T., MAJUMDAR, S., et al. Design of a wide band Frequency Selective Surface (FSS) for multiband operation of reflector antenna. In *The 5th International Conference on Computers and Devices for Communication (CODEC)*. Kolkata (India), 2012, p.1–3. DOI: 10.1109/CODEC.2012.6509202

[9] BISWAS, A. N., BALLAV, S., PARUI, S. K., et al. A polarization insensitive frequency selective surface with bandpass and bandstop response. In *IEEE Indian Conference on Antennas and Propagation*. Hyderabad (India), 2018, p. 1–4. DOI: 10.1109/INCAP.2018.8770800

[10] PEDDAKRISHNA, S, KHAN, T., KANAUJIA, B. K. Resonant characteristics of aperture type FSS and its application in directivity improvement of microstrip antenna. *AEU-International Journal of Electronics and Communications*, 2017, vol. 79, p. 199–206. DOI: 10.1016/J.AEUE.2017.06.007

[11] KAZEMZADEH, A., KARLSSON, A. Multilayered wideband absorbers for oblique angle of incidence. *IEEE Transactions on Antennas and Propagation*, 2010, vol. 58, no. 11, p. 3637–3646. DOI: 10.1109/TAP.2010.2071366

[12] PASIAN, M., MONNI, S., NETO, A., et al. Frequency selective surfaces for extended bandwidth backing reflector functions. *IEEE Transactions on Antennas and Propagation*, 2010, vol. 58, no. 1, p. 43–50. DOI: 10.1109/TAP.2009.2036185

[13] GURGEL DA SILVA SEGUNDO, F. C., PEREIRA DE SIQUEIRA CAMPOS, A. L., GOMES NETO, A. A design proposal for ultrawide band frequency selective surface. *Journal of Microwaves, Optoelectronics and Electromagnetic Applications*, 2013, vol. 12, no. 2, p. 398–409. DOI: 10.1590/S2179-10742013000200012

[14] CRUZ, R. M. S., D'ASSUNCAO, A. G., DA F. SILVA, P. H. A new FSS design proposal for UWB applications. In *2010 International Workshop on Antenna Technology* (iWAT). Lisbon (Portugal), 2010, p.1–4. DOI: 10.1109/IWAT.2010.5464645

[15] SOHAIL, I., RANGA, Y., ESSELLE, K. P., et al. A frequency selective surface with a very wide stop band. In *2013 7th European Conference on Antennas and Propagation (EuCAP)*. Gothenburg (Sweden), 2013, p. 2146–2148. ISBN: 978-88-907018-1-8

[16] RANGA, Y., MATEKOVITS, L., WEILY, A. R., et al. A low-profile dual-layer ultra-wideband frequency selective surface reflector. *Microwave and Optical Technology Letters*, 2013, vol. 55, no. 6, p. 223–1227. DOI: 10.1002/MOP.27583

[17] RAFIQUE, U., AGARWAL, S. A modified frequency selective surface band-stop filter for ultra-wideband applications. In *2018 International Conference on Advances in Computing, Communications and Informatics (ICACCI)*. Bangalore (India), 2018, p.1653–1656. DOI: 10.1109/ICACCI.2018.8554690

[18] FENG, D., ZHENG SHENQUAN, DINGFAN, et al. A n-order ultra-wideband frequency selective surface. IN *2016 11th International Symposium on Antennas, Propagation and EM Theory (ISAPE)*. Guilin (China), 2016, p. 648–651. DOI: 10.1109/ISAPE.2016.7834071

[19] CHATTERJEE, A., PARUI, S. K. A multi-layered broadband frequency selective surface for X and Ku band applications. In *Proceedings of the International Conference on Technical and Managerial Innovation in Computing and Communications in Industry and Academia*, 2013, p. 284–287.

[20] LUUKKONEN, O., COSTA, F., SIMOVSKI, C. R., et al. A thin electromagnetic absorber for wide incidence angles and both polarizations. *IEEE Transactions on Antennas and Propagation*, 2009, vol. 57, no. 10, p. 3119–3125. DOI: 10.1109/TAP.2009.2028601

[21] COSTA, F., MONORCHIO, A., MANARA, G. An overview of equivalent circuit modelling techniques of frequency selective surfaces and metasurfaces. *Applied Computational Electromagnetics Society (ACES) Journal,* 2014, vol. 29, no. 12, p. 960–976.

[22] GHOSH, S., SRIVASTAVA, K. V. An equivalent circuit model of FSS-based metamaterial absorber using coupled line theory. *IEEE Antennas and Wireless Propagation Letters*, 2015, vol. 14, p. 511–514. DOI: 10.1109/LAWP.2014.2369732

[23] DEWANI, A. A., O'KEEFE, S. G., THIEL, D. V., et al. Window RF shielding film using printed FSS. *IEEE Transactions on Antennas and Propagation*, 2018, vol. 66, no. 2, p. 790–796. DOI: 10.1109/TAP.2017.2780893

[24] LIU, C., XIANG, AN. A SIW-DGS wideband bandpass filter with a sharp roll-off at upper stopband. *Microwave and Optical Technology Letters*, 2017, vol. 59, no. 4, p. 789–792. DOI: 10.1002/MOP.30398

[25] SALMAN, J. W., MUDHAFFER, M. A., HASSAN, S. O. Effects of the loss tangent, dielectric substrate permittivity and thickness on the performance of circular microstrip antennas. *Journal of Engineering and Sustainable Development*, 2006, vol. 10, no. 1, p. 1–13. ISSN: 1813-7822

[26] ZHAI, H., ZHAN, C., LI, Z., et al. A triple-band ultrathin metamaterial absorber with wide-angle and polarization stability. *IEEE Antennas and Wireless Propagation Letters*, 2015, vol. 14, p. 241–244. DOI: 10.1109/LAWP.2014.2361011

[27] ABBASI, S., NOURINIA, J., GHOBADI, C., et al. A sub-wavelength polarization sensitive band-stop FSS with wide angular response for X-and Ku-bands. *AEU-International Journal of Electronics and Communications*, 2018, vol. 89, p. 85–91. DOI: 10.1016/J.AEUE.2018.03.018

About the Authors ...

Anik Naha BISWAS received the B.Tech. degree in Electronics and Communication Engineering from Maulana Abul Kalam Azad University of Technology, West Bengal, India and M.Tech degree in Microwave and Communication Engineering from Indian Institute of Engineering Science and Technology, Shibpur, India in the year 2017 and 2019, respectively. He is currently pursuing Ph.D. degree in Microwave Engineering at School of Electrical and Electronics Engineering, Nanyang Technological University, Singapore since August 2019.

Suparna BALLAV received the B.Sc. (Physics Hons) degree in 2011 and the B.Tech. and M.Tech in Radio Physics and Electronics from University of Calcutta, India in the year 2014 and 2016, respectively. She is pursuing Ph.D. degree in Microwave Engineering at the Department Electronics and Tele-communication Engineering, Indian Institute of Engineering Science and Technology (IIEST), Shibpur, West Bengal, India since August 2016. Her research interests include dielectric resonators for microwave circuits and antenna application.

Ayan CHATTERJEE was born in West Bengal, India, in 1988. He received the B.Tech. degree in Electronics and Communication Engineering from the West Bengal University of Technology, India, in 2010 and the M.Tech. degree in Communication Engineering from University of Kalyani, West Bengal, India, in 2012. From 2012 to 2013, he was an Assistant Professor with the Electronics and Communication Engineering Department, SKFGI, West Bengal, India. In 2018, he has completed his Ph.D. degree in Microwave Engineering at the Electronics and Tele-Communication Engineering Department, Indian Institute of Engineering Science and Technology, Shibpur, West Bengal, India. He is the author of more than 17 papers in referred journals and conference proceedings. His research interests include frequency selective surfaces for radome and antenna systems. Mr. Chatterjee received Senior Research Fellowship from the Council of Scientific and Industrial Research, Govt. of India in 2014. He also received Best Paper Award in CCSN, Rourkela, India in 2013 and in RSC, IIEST Shibpur in 2016.

Susanta Kumar PARUI received the B.Sc. degree in Physics and B.Tech. degree in Radio Physics and Electronics from University of Calcutta, India in the year 1987 and 1990, respectively and the Ph. D. degree in Microwave Engineering from Bengal Engineering and Science University (presently known as Indian Institute of Engineering Science and Technology), Shibpur, India. From 1993 to 2000, he was an Instrument Engineer in process control industries. Since 2000, he has been associated with the Department of Electronics and Tele-Communication Engineering, Indian Institute of Engineering Science & Technology, Shibpur and presently holds the post of Associate Professor. He is the author of more than 60 papers in referred journals and conference proceedings. His research interests include planar circuits, antennas, SIW, DGS, EBG, FSS and Metamaterials. Dr. Parui was awarded postdoctoral fellowship from the Royal Academy of Engineering, U.K in the year 2009.